

A Monte Carlo simulation of the interactions of cosmic rays with the atmosphere

P. Zuccon¹, B. Bertucci¹, B. Alpat¹, R. Battiston¹, G. Battistoni², W. J. Burger¹,
G. Esposito¹, A. Ferrari^{2,3}, E. Fiandrini¹, G. Lamanna¹, P. Sala^{2,3}

September 14, 2001

¹ Università and Sezione INFN of Perugia, Italy

² Sezione INFN of Milano, Italy

³ CERN Switzerland

Abstract

Substantial fluxes of protons and leptons with energies below the geomagnetic cutoff have been measured by the AMS experiment at altitudes of 370-390 Km, in the latitude interval $\pm 51.7^\circ$. The production mechanisms of the observed trapped fluxes are investigated in detail by means of the FLUKA Monte Carlo simulation code. All known processes involved in the interaction of the cosmic rays with the atmosphere (detailed descriptions of the magnetic field and atmospheric density, as well as the electromagnetic and nuclear interaction processes) are included in the simulation. The results are presented and compared with the experimental data, indicating good agreement with the observed fluxes. The impact of secondary proton flux on particle production in atmosphere is briefly discussed.

1 Introduction

Cosmic rays approaching the Earth interact with the atmosphere resulting in a substantial flux of secondary particles. A reliable estimate of the secondary flux composition and energy spectra is of considerable interest, e.g. the evaluation of background radiation for satellites and the estimate of the atmospheric neutrino production for neutrino oscillation experiments [4].

The accurate AMS measurements of charged fluxes of cosmic and secondary particles in the near Earth region allow an extensive test of models describing the cosmic ray interactions with the atmosphere and the evolution of the produced secondary particles in the magnetic field.

In this work, we report results from a Monte Carlo simulation based on FLUKA 2000 [8], which describes the interaction of the cosmic protons with the Earth's atmosphere, including the propagation of the secondaries in the Earth's magnetic field.

2 The model

An isotropic flux of protons is uniformly generated on a geocentric spherical surface with a radius of 1.07 Earth radii ($\sim 500 \text{ Km}$ a.s.l.) in the kinetic energy range $0.1 - 170 \text{ GeV}$.

The energy spectrum is modeled according to a power law, modified to account for the solar modulation effects as suggested in [11]. Both the spectral index and the solar modulation parameter are extracted from a fit of the AMS data [2].

The magnetic field in the Earth's proximity includes two components: the Earth's magnetic field, calculated using a 10 harmonics IGRF [14] implementation, and the external magnetic field, calculated using the Tsyganenko Model¹[15].

To account for the geomagnetic effects, for each primary proton we back-trace an antiproton of the

same energy until one of the following conditions is satisfied:

1. the particle reaches the distance of $10 E_R$ from the Earth's center.
2. the particle touches again the production sphere.
3. neither 1 or 2 is satisfied before a time limit is reached.

If condition 1 is satisfied the particle is on an allowed trajectory, while if condition 2 is satisfied the particle is on a forbidden one. Condition 3 arises for only a small fraction of the events $O(10^{-6})$.

Particles on allowed trajectories are propagated forward and can reach the Earth's atmosphere. The atmosphere around the Earth is simulated up to 120 Km a.s.l. using 60 concentric layers of homogeneous density and chemical composition. Data on density and chemical composition are taken from the standard MSIS model [12]. The Earth is modeled as a solid sphere which absorbs each particle reaching its surface.

2.1 The generation technique

The ideal approach in the generation of the primary cosmic rays spectra would be to start with an isotropic distribution of particles at a great distance (typically $10 E_R$) from the Earth where the geomagnetic field introduces negligible distortions on the interstellar flux. However, this computational method is intrinsically inefficient since most of the particles are generated with trajectories which will not reach the Earth environment. Kinematical cuts can be applied in order to improve the selection efficiency at generation, however they tend to introduce a bias for low rigidities particles.

A good alternative to this approach is the back-tracing method [13] [6] adopted in the present analysis as outlined in the previous section. In the following, we will shortly discuss the validity of the

¹The external magnetic field is calculated only for distances greater than 2 Earth's radii(E_R) from the Earth's center

technique and report the results of a comparison of the two methods. We recall that this method was applied for the first time in ref. [7] for the generation of atmospheric neutrino fluxes.

Let us consider first the effects of the geomagnetic field on an incoming flux of charged particles in the absence of a solid Earth. For the discussion, we start with an isotropic flux of monoenergetic² protons at large distance, i.e. at infinity, from the origin of a geocentrical reference system. In this scenario, a negligible fraction of particles, with very particular initial kinematic parameters, will follow complicated paths and remains confined at a given distance from the origin (semi-bounded trajectories); for all practical purposes this sample can be ignored. Most of the particles will follow unbounded trajectories, reaching again infinity after being deflected by the magnetic field.

Unbounded trajectories cross a spherical surface centered in the field source only an even number of times, as shown in fig.1: we call *legs* the trajectory parts connecting the spherical surface to infinity and *loops* the parts of the trajectory starting and ending inside the spherical surface.

Since each trajectory can be followed in both directions and no source or sink of particles is contained within the surface, the incoming and outgoing fluxes are the same. However, the presence of the magnetic field breaks the isotropy of the flux “near” the field source, so for a given location there is a flux dependence due to the direction.

Applying the Liouville Theorem, under the hypothesis of isotropy at infinity, it is straightforward to prove [10] that the proton flux in a random point is the same as at infinity along a set of directions (allowed directions), and zero along all the others (forbidden directions).

The pattern of the allowed and forbidden directions depends on both the rigidity and the location and is known as the geomagnetic cutoff.

With the introduction of a solid Earth, all the tra-

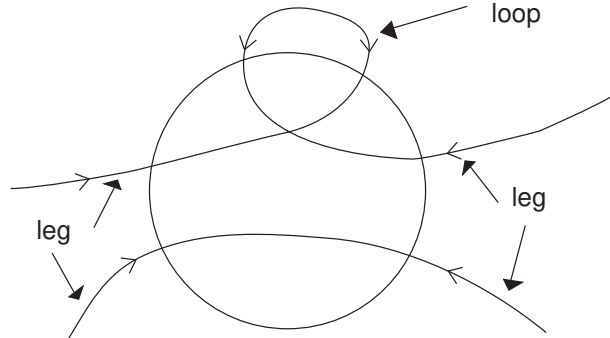


Figure 1: Trajectories types crossing a spherical surface around the Earth

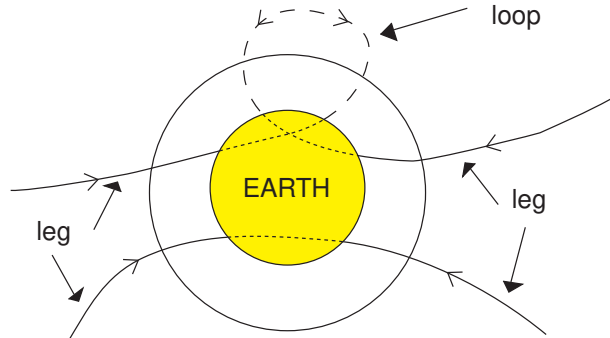


Figure 2: Trajectories in the presence of a solid Earth

jectories that are crossing the Earth are broken in two or more pieces (fig.2): the *legs* become one-way trajectories and the *loops* disappear.

The presence of the Earth modifies the flux which exits from the surrounding spherical surface, since particles are absorbed by the Earth, while it has only a minimal effect on the incoming flux which is modified only by the absence of certain *loops*.

To generate the flux of particles reaching the Earth’s atmosphere, it is sufficient to follow the particles along the allowed trajectories corresponding to the *legs*, taking care to avoid double or multiple counting.

To respect this prescription we reject all trajectories that are back-traced to the production sphere, this allow us to correctly consider the cases like the one shown in fig.3.

We point out that an important difference with

²The realistic case of an energy spectrum can be treated just as a superposition of monenergetic cases

respect to the application in the neutrino flux calculation of [7] is that for the former, the generation sphere coincided with the Earth's surface, and therefore the forbidden trajectories included those which touched again the Earth (plus those who remained trapped for a long time). In that case there are no problems of double counting.

To check the validity of our technique we made a test comparing the results of the “brute force” generation technique at 10 Earth's radii distance from the Earth's center with the backtracing technique described in this paper.

Figure 4 shows this comparison for several characteristic distributions, the agreement between the two methods is good.

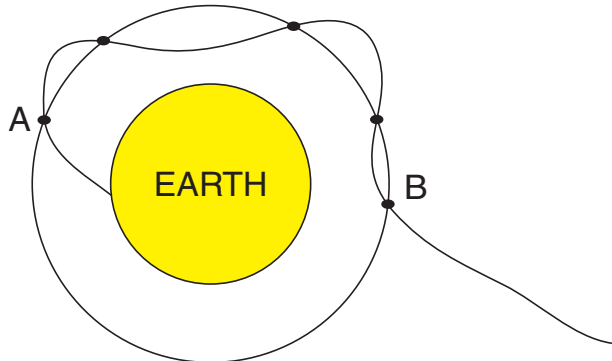


Figure 3: An example of multiple counting along a trajectory, this type of trajectory has to be considered only at point B.

2.2 The interaction model

We use the software package FLUKA 2000 [8] to transport the particles and describe their interactions with Earth's atmosphere. This package contains a tridimensional description of the interactions and should reproduce the spatial distribution of secondaries better than older models based on empirical parameterizations of accelerator data.

Interactions are treated in a theory-driven approach, and the models and their implementations are guided and checked using experimental data. Hadron-nucleon interaction models are based on

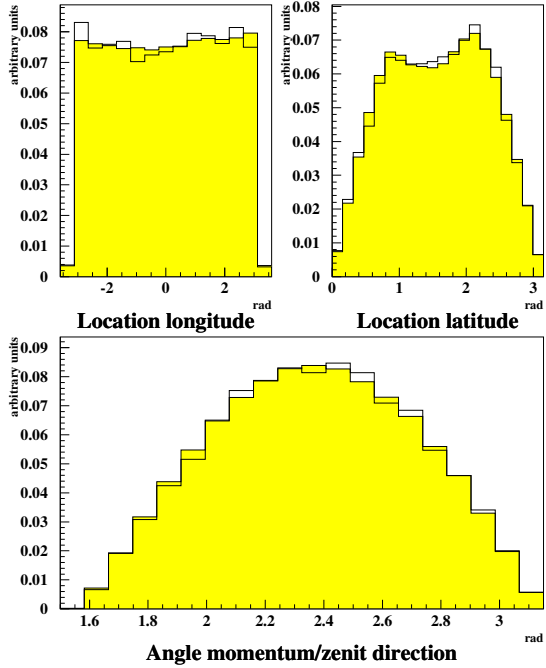


Figure 4: Latitude and longitude of impact points and angle between momentum and zenith directions for particles generated at a distance of 10 Earth's radii (solid line) and particle generated at 1.07 Earth's radii (shaded histogram).

resonance production and decay below an energy of few GeV and on the Dual Parton Model above.

The extension to hadron-nucleus interactions is done in the framework of a generalized intra-nuclear cascade approach including the Gribov-Glauber multi-collision mechanism for higher energies followed by equilibrium processes: evaporation, fission, Fermi break-up and γ de-excitation.

In fig 5 a) we show the map of the primary proton interaction points in geographical coordinates. The distribution reflects the influence of the geomagnetic cutoff. Fig 5 b) shows the interactions altitude profile, the solid histogram is for $E_k < 30 GeV$ while the dashed one is for $E_k > 30 GeV$. The mean interaction altitude depends weakly on the energy.

In tab.1 we list the characteristic features of the

	$E_k < 30 \text{ GeV}$	$E_k > 30 \text{ GeV}$
Elastic interactions	26%	24%
Inelastic interactions	74%	76%
Average mult. of ch. secondaries	5	11

Table 1: Characteristics of the cosmic protons interactions with atmosphere

cosmic proton interactions in the atmosphere.

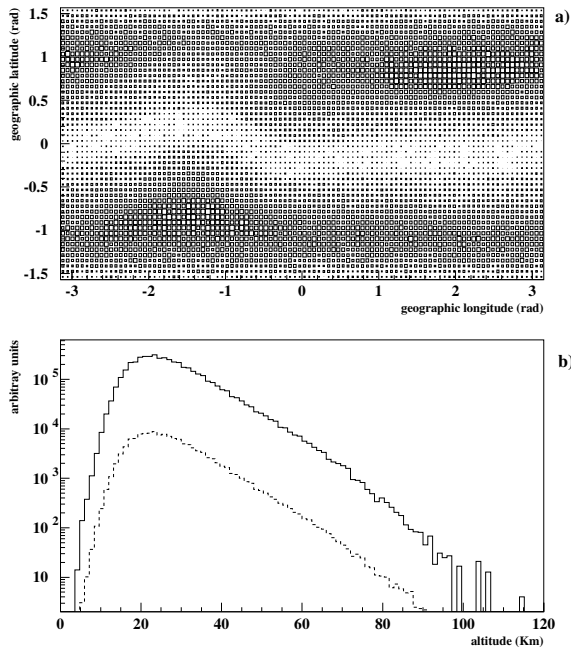


Figure 5: a) distribution of primary protons interaction points in geographical coordinates, b) altitude profile of primary protons interaction points, solid line $E_k < 30 \text{ GeV}$, dashed line $E_k > 30 \text{ GeV}$

3 Comparison with the AMS data

To compare with the AMS data, we define a detection boundary corresponding to a spherical surface at the AMS orbit altitude (400 Km a.s.l).

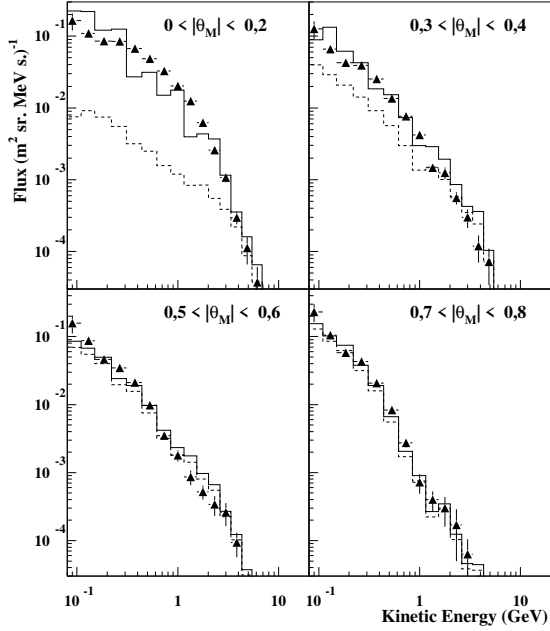


Figure 7: Upgoing proton fluxes, simulation (solid line) and the AMS data (triangles); the dashed lines are described in the text.

We record each particle that crosses the detection boundary within the AMS field-of-view defined as a cone with a 32 degree aperture with respect to the local zenith or nadir directions.

To obtain the absolute normalization, we take into account the field-of-view, the corresponding AMS acceptance, and an *equivalent time exposure* (E.T.E) corresponding to the number of primary protons generated.

Our results are based on a sample of $\sim 3 \cdot 10^6$ primary protons generated in the kinetic energy range of $0.1 - 170 \text{ GeV}$, which corresponds to $\sim 1 \cdot 10^{-12} \text{ s}$ (E.T.E).

3.1 Protons

In fig.6, we show the comparison between the fluxes obtained with the simulation and the measured AMS downgoing proton flux [1] in nine bins of geomagnetic latitude (θ_M). Fig.7 shows the

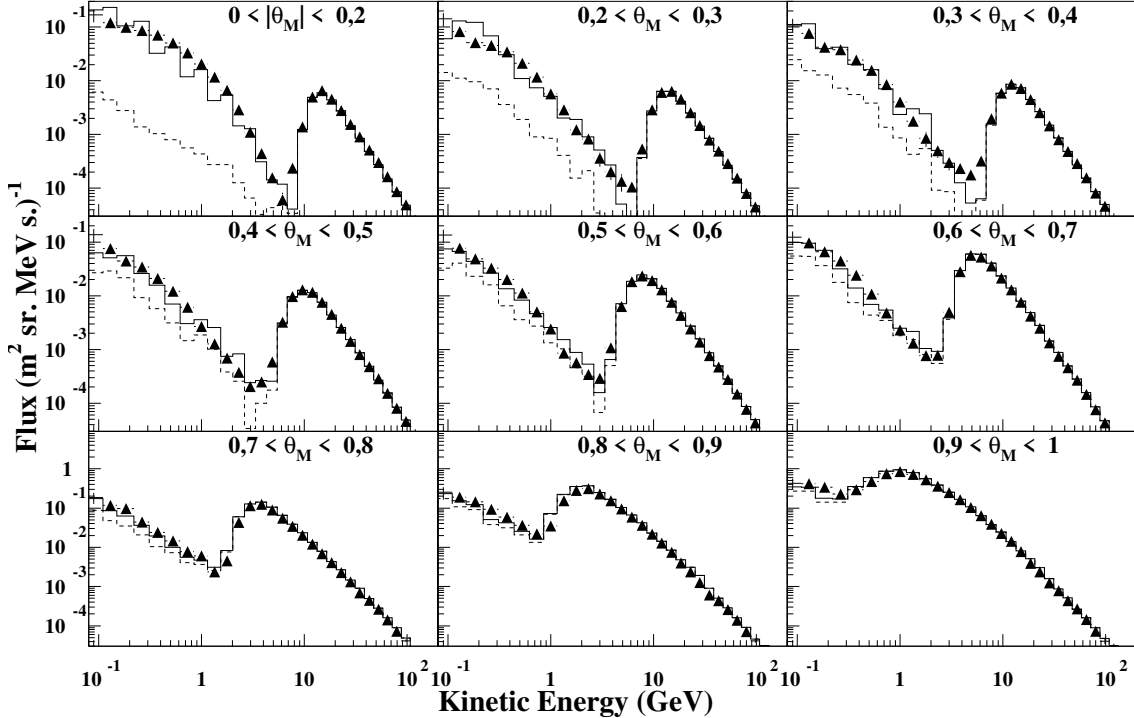


Figure 6: Downgoing proton flux, simulation(solid line) and the AMS data (triangles); the dashed lines are described in the text. Θ_M is the geomagnetic latitude in radians.

same comparison for the upgoing proton flux in four selected θ_M bins.

As seen in fig.6, the simulation reproduces well at all latitudes, the high energy part of the spectrum and the falloff in the primary spectrum due to the geomagnetic cutoff, thus validating the general approach used for the generation and detection, as well as the tracing technique.

The part of the spectrum below the geomagnetic cutoff is sensitive to the interaction model. In particular, it is populated by the low energy protons produced in primary interactions with the atmosphere and that spiral along the field lines in the vicinity of the detecting altitude.

Their number and energy distribution depend on the details of the target fragmentation model. The results depend also on the accuracy of the particle transport algorithm and on the details of the at-

mosphere description. The results shown in figs. 6 and 7 were obtained with FLUKA2000[8] code, making use of a setup derived from the one adopted in [4].

In figs. 6 and 7, the bin-to-bin statistical fluctuations are seen at the lower kinetic energies, particularly in the equatorial region. This part of the spectra corresponds to the undercutoff component where the observed flux is the result of multiple detections of the same particles. The importance of the effect on the observed fluxes is illustrated by the *real proton flux*, i.e. the flux obtained by counting only once each particle crossing the detector, which is indicated by the dashed distributions in figs. 6 and 7. In particular, the *real number* of protons crossing the detector in the equatorial region is more than one order of magnitude lower than the observed flux. As a consequence statistical fluctu-

ations of the simulated data are amplified by this effect.

At high geomagnetic latitudes, the solid and dashed lines merge. The effect becomes negligible for $\theta_M > 0.8$.

Within the formalism of adiabatic invariants, it is seen that trapped particles, i.e. the undercutoff protons, move along drift shells which can be associated with a characteristic residence time³ that depends on the fraction of the shell located inside the Earth's atmosphere. Thus, particles moving along *long-lived* shells have a large probability to cross many times a geocentered spherical detector, while those moving along *short-lived* shells typically cross the detector one time.

The drift shells crossing the AMS orbit, at an altitude of 400 km, are in general *short-lived*, however in the equatorial region the *long-lived* are present as well.

In consequence, the “real” undercutoff component of the protons fluxes is at least one order of magnitude lower than the primary CR proton component at all latitudes, even in the equatorial region where the AMS measurement indicates an important secondary proton flux. This can be better seen in fig.8, where the integral primary proton flux seen by AMS is shown as a function of geomagnetic latitude. The intensities of the “real” and measured undercutoff fluxes are reported in the same plot for comparison and their ratio with the primary component shown in fig.9. A minor contribution from the undercutoff proton component can be therefore expected in the atmospheric shower development and neutrino production.

In figure 10, the life time is plotted versus the kinetic energy of the trapped secondary protons for $|\theta_M| < 0.4$. In the scatter plot it is possible to distinguish the populations corresponding to *long-lived* and *short-lived* shells similar to those shown in [3] for leptons.

Fig.11 shows the distribution of trapped sec-

ondary proton end points for $|\theta_M| < 0.4$, fig.11a is for a lifetimes smaller than 0.3 s., while fig.11b is for a lifetimes greater than 0.3 s.. The end point distribution agrees with the location of the intersections of the drift shells with the atmosphere as experimentally verified by [1], and discussed in [9].

3.2 Electrons and positrons

In fig. 12 we show a comparison of the simulated undercutoff electron and positron downgoing fluxes with the corresponding AMS measured fluxes [3]. The AMS positron measurement is limited to energies below 3 GeV , corresponding to the upper limit of proton rejection of the threshold Cherenkov counter used to distinguish protons and positrons.

In fig.13b-c we show the integrated positron and electron downgoing fluxes for the kinetic energy range 0.2–1.5 GeV as a function of θ_M . The simulation reproduces reasonably well the general behavior of the data in terms of shape and intensity; a similar agreement is observed for the upgoing lepton spectra (not shown).

As in the case of protons, statistical fluctuations affect the comparison in the equatorial region. The *real lepton fluxes*, corresponding to the *real proton flux* described earlier, are shown as the dashed line distributions in fig. 12

An interesting feature of the comparison is the fact that in the equatorial region, the electrons are produced essentially by primary protons with $E_k > 30 GeV$, while for the positrons lower energy protons contribute as well. This distinction disappears at higher latitudes. This behavior can be explained by the East-West asymmetry of the geomagnetic cutoff. Westward-moving protons produce positrons which will populate the drift shells, while the produced electrons enter the atmosphere [5]. The energy spectrum of eastward-moving protons is affected by the geomagnetic cutoff. As a consequence, the interacting protons in the equatorial region have higher energies (lower flux) yield-

³The mean time after which a particle is absorbed into the atmosphere.

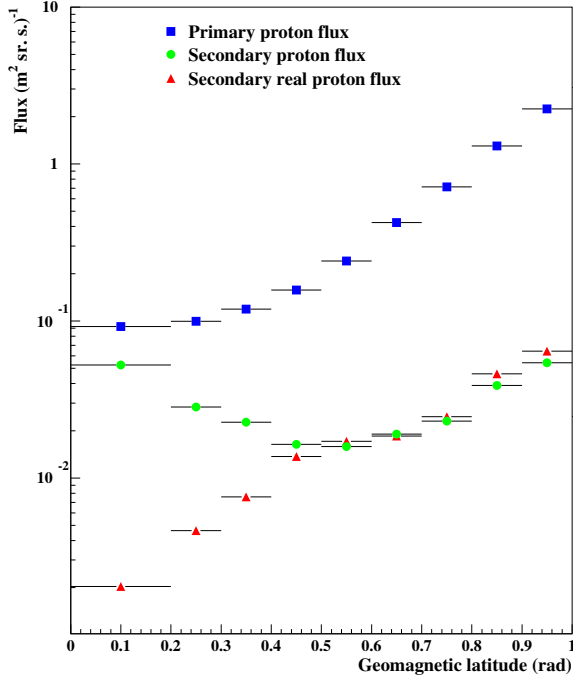


Figure 8: Proton fluxes seen AMS as calculated with this simulation, as function of the geomagnetic latitude. The fluxes are integrated over the kinetic energy range $0.1 - 170 \text{ GeV}$.

ing a lower undercutoff electron flux compared to the undercutoff positron flux.

4 Conclusion

Our results show good agreement between simulation and the measured data. The Monte Carlo simulation describes well the undercutoff proton and lepton fluxes. Our results indicate that the undercutoff proton flux should have a small impact on secondary particle production in the atmosphere. However this will be object of further and more refined study in the future.

The simulation, constrained by the high statistic measurements of AMS, can be used to assess the radiation environment in near-Earth orbit,

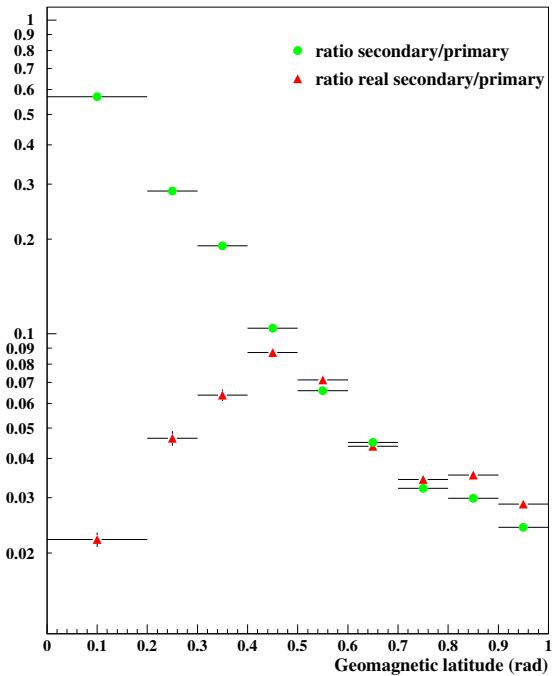
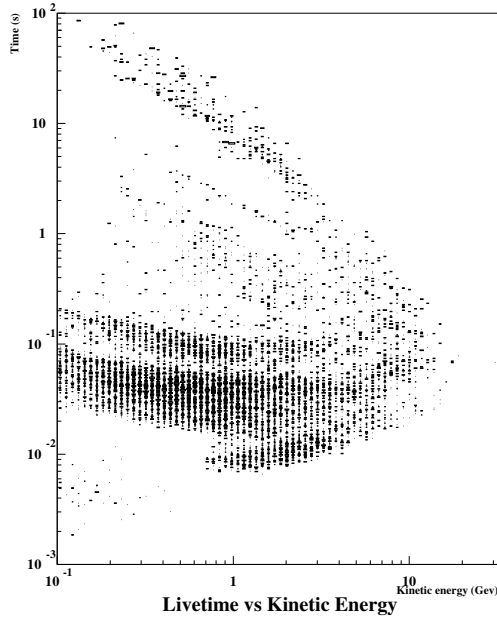


Figure 9: Ratios of the fluxes shown in fig.8

and represent a valuable tool for more accurate calculations of particle fluxes in atmosphere.

This work has been partially supported by the Italian Space Agency (ASI) under contract ARS-98/47.



Livetime vs Kinetic Energy

Figure 10: Life time versus kinetic energy for secondary protons produced in the interactions of primary cosmic rays with the atmosphere. The protons are detected at geomagnetic latitude $|\theta_M| < 0.4$ rad.

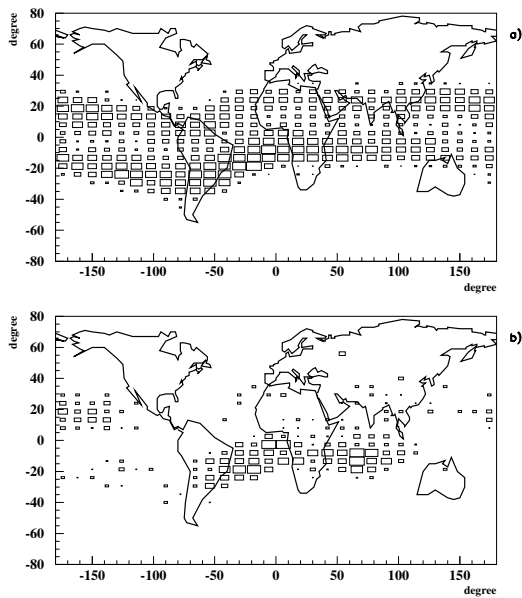


Figure 11: Maps of secondary protons end points for geomagnetic latitude $|\theta_M| < 0.4$ rad. Figure (a) live time < 0.3 s Figure (b) live time > 0.3 s

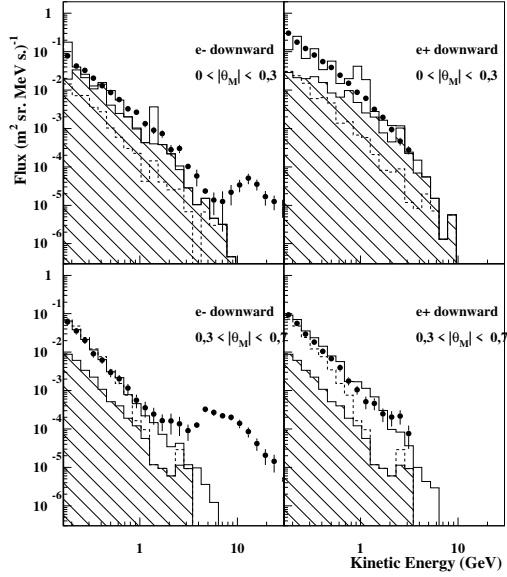


Figure 12: Downgoing positron and electron fluxes in two regions of geomagnetic latitude θ_M , solid histogram (simulation) black points (AMS data); hatched histogram shows the positron and electron fluxes produced by primary protons with $E_k > 30$ GeV; the dashed line distributions are described in the text.

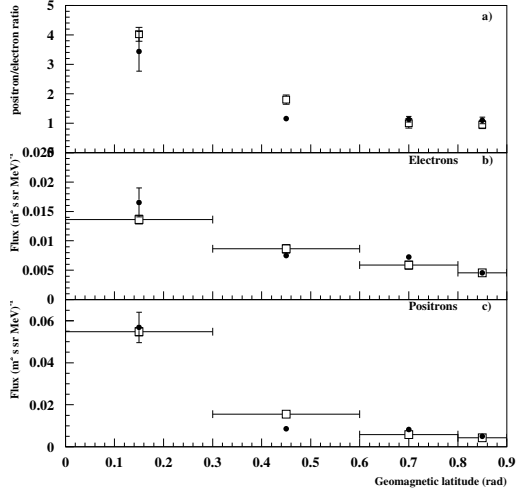


Figure 13: Electron (b) and positron (c) fluxes and their ratio (a) integrated in the kinetic energy range $0.2 - 1.5$ GeV, as function of geomagnetic latitude. Open squares (AMS data), black points (simulation).

References

- [1] J.Alcaraz et al.,AMS Collaboration, Protons in Near Earth Orbit, Phys.Lett. B472, 215-226, 2000 (a).
- [2] J.Alcaraz et al.,AMS Collaboration, Cosmic Protons, Phys. Lett. B490, 27-35, 2000 (b)
- [3] J.Alcaraz et al.,AMS Collaboration, Leptons in Near Earth Orbit, Phys.Lett. B484, 10-22, 2000 (c).
- [4] G. Battistoni et al., Astroparticle Physics 12,315-333, 2000. Numerical results are obtainable at <http://www.mi.infn.it/~battist/neutrino.html>.
- [5] L.Derome et al., Origin of leptons in near earth orbit, astro-ph/0103474, 2001.
- [6] L. Derome, et al. “Origin of the high-energy proton component below the geomagnetic cutoff in near Earth orbit” Phys. Lett. B489, 1-8, 2000
- [7] M. Honda et al., Phys. Rev. D52 4985, 1995.
- [8] A. Ferrari et al., The FLUKA radiation transport code and its use for space problems, Proceedings of the “1 st International Workshop on Space Radiation Research and 11 th Annual NASA Space Radiation Health Investigators’ Workshop”, Arona (Italy), May 27-31, 2000, Physica Medica, Vol XVII, Suppl. 1.
- [9] E. Fiandrini et al. ‘Leptons with $E > 200\text{MeV}$ trapped in the Earth’s radiation belts’, ICRC 2001 proceedings.
- [10] M.S.Vallarta “Theory of the Geomagnetic Effects of Cosmic Radiation” published in the Encyclopedia “Handbook der Physik” Vol. XLVI.
- [11] L.J. Gleeson and W.I.Axford, Astroph. Journal 154, p11011,1968
- [12] A. E. Hedin, Extension of the MSIS Thermo-spheric Model into the Middle and Lower Atmosphere, J. Geophys. Res. 96, 1159, 1991.
- [13] P.Lipari, The fluxes of subcutoff particles detected by AMS, the cosmic ray albedo and atmospheric neutrinos, astro-ph/0101559, 2001.
- [14] N.A. Tsyganenko Geomagn. and Aeronomy (1986), V.26, P.523-525; N.A. Tsyganenko and M.Peredo, Geopack Manual,(1992)
- [15] N.A. Tsyganenko and D.P. Stern, A new-generation global magnetosphere field model , based on spacecraft magnetometer data, ISTP newsletter, v.6, no.1, p.21, feb.1996.